Arch-shaped Triboelectric Nanogenerator with Ni/Cu Bimetallic MOF-engineered Intermediate layer for Self-Powered Electrochemical Clean Hydrogen Production and Environmental Remediation

*Debmalya Sarkar[1], Manaswini Ravipati[1], Richa Kumari[2], Sushmee Badhulika[1]**

[1] Department of Electrical Engineering, Indian Institute of Technology Hyderabad, India.

[2] Department of Physics, Institute of Science, Banaras Hindu University Varanasi, 221005, Uttar Pradesh, India

*Corresponding author E-mail address: sbadh@iith.ac.in

S1. Experimental

S1.1 Materials and Reagents

The analytical grade reagents such as Nickel Chloride Hexahydrate ($NiCl_2 \cdot 6H_2O$, 97%), Cupric Acetate Monohydrate ($(CH_3COO)_2Cu \cdot H_2O$, 98%), Trimesic Acid or 1,3,5-benzenetricarboxylic acid (BTC, $C_6H_3(CO_2H)_3$, 98%), dimethylformamide (DMF), and ethanol (99.8%) were purchased from Sigma Aldrich, BLD Pharmatech (India) and SRL India. Deionized water (DI) was taken from a Millipore system with a resistivity of 18.2 MΩ cm^{-1}. The nylon cloth, PDMS and ecoflex were collected from the nearby local shops. The copper electrode (thickness of 250 µm, resistance 0.3 ohms for 5 cm X 2.3 cm) and carbon tape (thickness of 160 µm and resistance 5 ohms/sq) were purchased from an online shopping platform.

S1.2 Synthesis of Ni/Cu bimetallic MOF

The bimetallic Ni/Cu-MOF was synthesized via a facile solvothermal route. In detail, BTC (46.5 mM), copper acetate monohydrate (46.6 mM), and nickel chloride hexahydrate (46.0 mM) were dissolved in a mixed solvent consisting of 35 mL DMF, 4 mL ethanol, and 4 mL deionized water to form a homogeneous solution. The resulting mixture was transferred to a 50 mL Teflon-lined stainless-steel autoclave and heated at 100°C for 10 h to yield the Ni/Cu-MOF material. After heating, the mixture was cooled down to room temperature and centrifuged at 6000 rpm for 5 minutes. The clear liquid on top was carefully poured off, and the solid was re-dispersed in DI water and ethanol then centrifuged. This washing step was repeated 2-3 times to remove unreacted materials. The final solid was dried overnight at 70°C and then gently ground with a mortar and pestle to obtain a fine powder of Ni/Cu-MOF.

S1.3. Instruments

The Surface morphologies of the synthesized bimetallic MOF were investigated using scanning electron microscopy (SEC SNE 3200M). The Structural properties were further examined by a line on X' pert PRO X-ray diffraction (XRD) with Cu Kα1 radiation (λ = 1.54 Å). Moreover, the Fourier-transform infrared spectroscopy (FTIR) (Bruker Alpha spectrometer) was used to see the functional group of the as-synthesized material and intermediate layer. The dielectric measurement was performed using an LCR meter SM6019. Additionally, the elemental composition and chemical states of the metal centers were determined using X-ray

photoelectron spectroscopy (XPS, Axis Supra, Kratos Analytical) equipped with a non-monochromated Al Kα X-ray source (hν = 1.4866 keV). During the analysis of the surface potential through KPFM, the antimony-doped Si cantilever was used as a probe. For the scan, the scan size and scan angle were 500 nm and 0^0, respectively. Also, the room temperature was maintained throughout the whole experiment. Moreover, the electrical properties of the fabricated NCIL-TENG were measured by using a source meter (Keithley, Tektronix, 2450). A digital storage oscilloscope (SDS 1104X-E) with a 10:1probe was used to collect the output voltage of the device.

S2. TGA analysis of MOF, investigating the role of MOF inside the PDMS matrix and monitoring the energy storage ability, durability and thermal dependency of the device

In this work, the Ni/Cu bimetallic MOF plays a pivotal role by delivering interfacial and localized electrical response, thereby improving the output performance of the fabricated device without compromising charge retention. Besides this, the bimetallic MOF has inherent but moderate electronic conductivity, arising from charge-transfer pathways involving metal-ligand interactions, redox-active metal centres, and partially delocalized electronic states. When we have incorporated the Ni/Cu MOF inside the PDMS matrix with an even distribution, below the percolation level, they remain electrically isolated from one another due to the insulating polymer matrix. During the contact-electrification process, the charges generated at the PDMS surface encounter an electric field that induces charge redistribution at the MOF-polymer interfaces. The intrinsic conductivity of the bimetallic MOF allows for rapid local charge movement and stabilization at these interfaces, leading to Maxwell-Wagner-Sillars (MWS) interfacial polarization that results in the accumulation of space charges at the interfaces. For this phenomenon, an enhancement is observed in the dielectric permittivity and capacitance of the Ni/Cu bimetallic MOF@PDMS composite, as shown in the figure S1 (a) and (b). Furthermore, charge transport in this system relies on capacitive coupling, interfacial polarization, and short-range hopping between localized interfacial states. During the contact-electrification process, this mechanism improves charge storage and reduces charge recombination, resulting in better electrostatic induction and output performance.

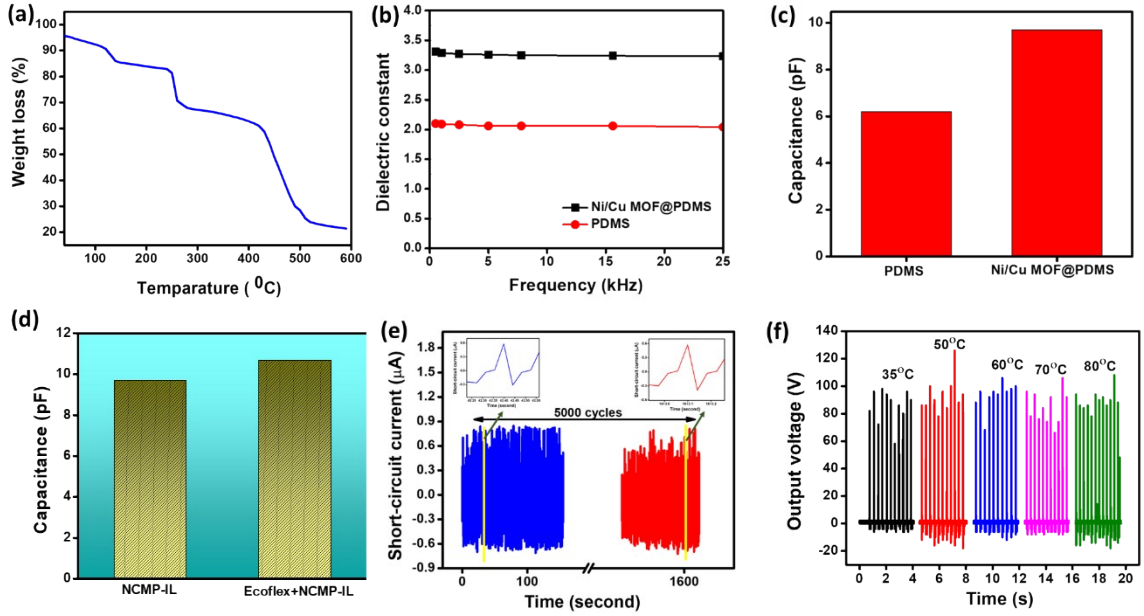

Figure S1: (a) Thermal analysis of the synthesized Ni/Cu MOF. Investigation of the (b) dielectric constant and (c) capacitance values of the pure PDMS and Ni/Cu MOF@PDMS composite. (d) Examining the energy storage ability of the NCMP-IL and NCMP-IL + ecoflex double layer in terms of the specific capacitance value. (e) Monitoring the durability of the fabricated NCIL-TENG device over 5000 cycles. (f) Investigating the influence of the different temperatures on the output voltage of the fabricated triboelectric device.

S3. Operating mechanism of the half-wave rectifying circuit during the connection with the NCIL-TENG

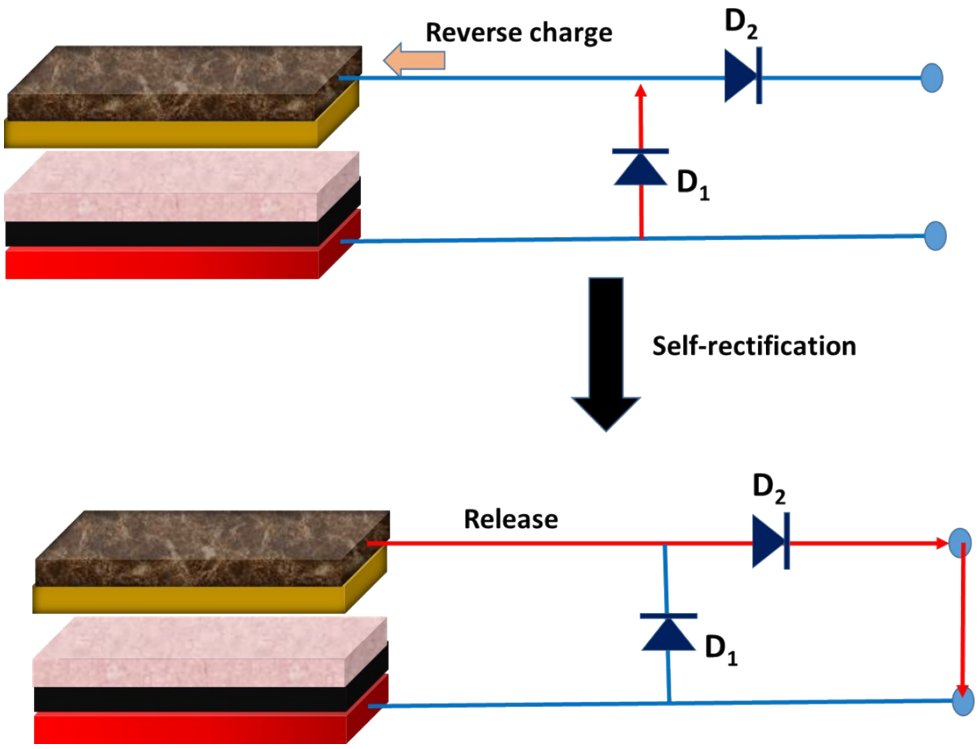

Figure S2. Schematic of the working mechanism of the half-wave rectifying circuit.

S4. Monitoring the output voltage before and after water splitting

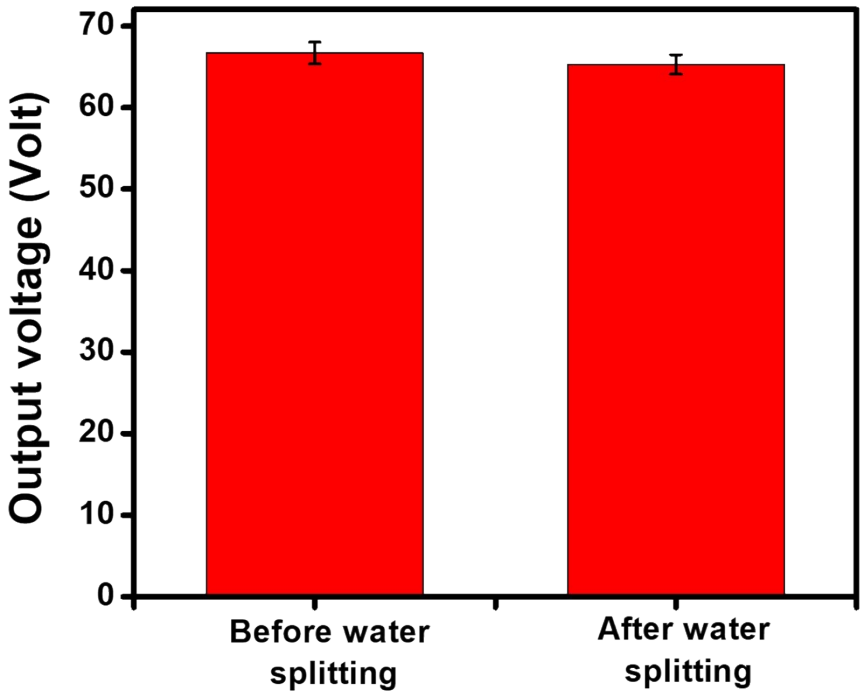

Figure S3: Monitoring the output voltage of the NCIL-TENG generated before and after the water splitting process.

S5. Monitoring the effect of the HWR setup on the degradation curves of the RhB

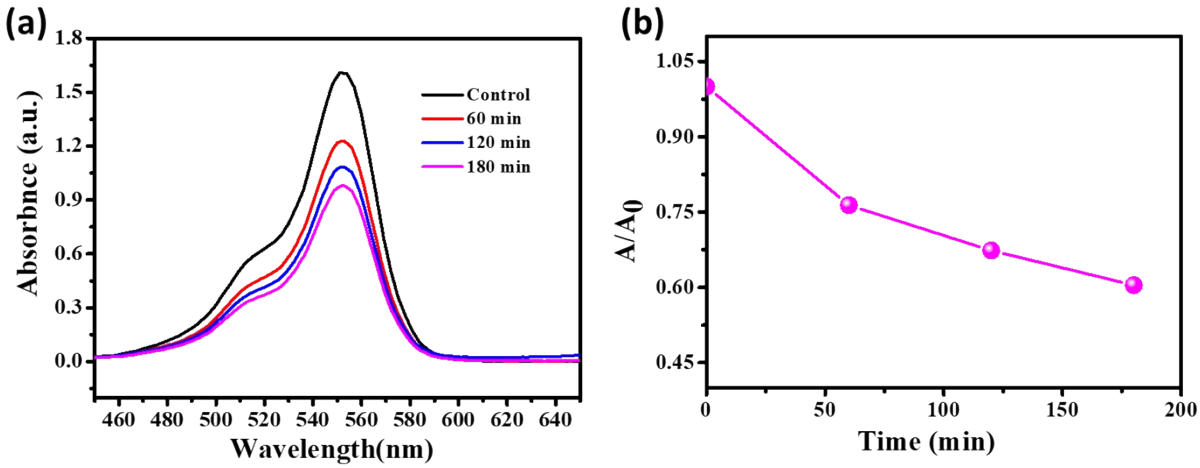

Figure S4: (a) Absorbance spectra of the RhB dye, showing the degradation over time. (b) Variation of RhB concentration with electrocatalytic degradation time.

S6. Degradation of atrazine performed by using the HWR set-up

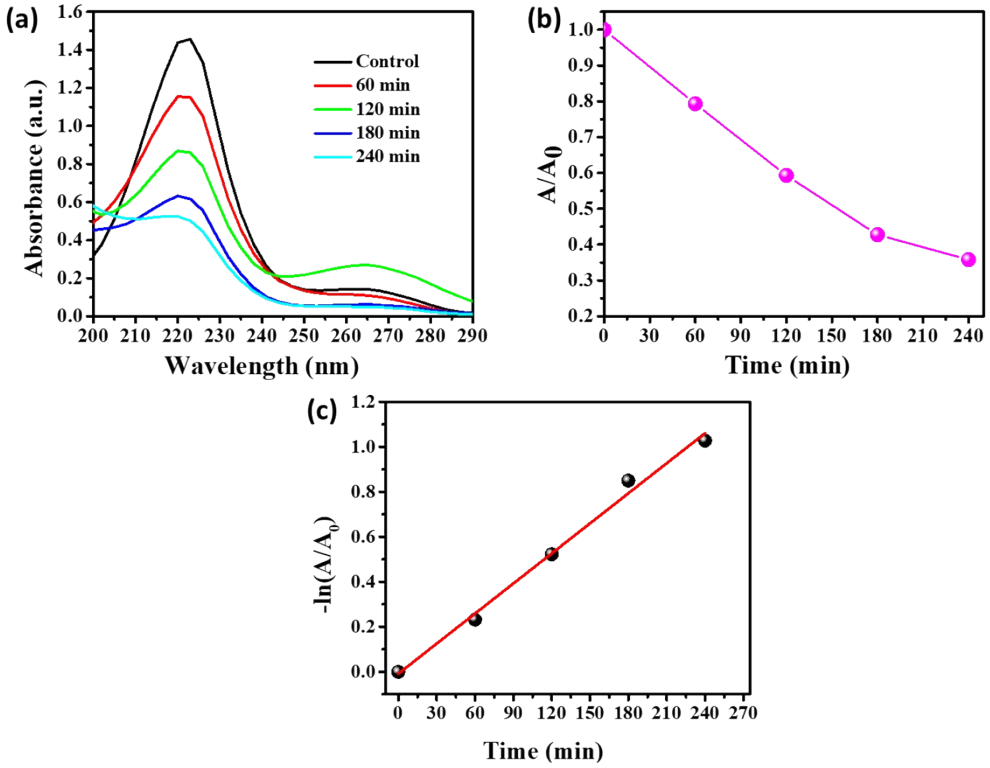

Figure S5: (a) Absorbance spectra of atrazine dye, showing the degradation over time. (b) Variation of atrazine concentration with electrocatalytic degradation time and (c) associated linear fitting kinetic curves.

S7. External force (F) calculation of the NCIL-TENG device

Using the following equations, the applied force on the NCIL-TENG device has been calculated under periodic finger tapping mode. Moreover, these two equations depend on the momentum and energy conservation law.[1]

$$m.g.h = \tfrac{1}{2}\, mv^2$$

$$\text{or, } v = (2gh)^{1/2}$$

$$(F-mg).\Delta t = m.v$$

Where m and v describe the mass of the imparted object, which means fingers and the velocity of the object when it touches the device, h is the falling height of the object, F is the applied

force, g is the acceleration due to gravity, and Δt describes the time duration between two peaks measured from the output graph.[1]

S8. Energy conversion efficiency of the triboelectric device

The mechanical energy conversion efficiency of the fabricated triboelectric device has been measured. By using the following equation[2], the efficiency has been calculated.

$$\eta_{mech} = \frac{E_{electric}}{E_{kinetic}} \times 100\ \%$$

During charging a 100 μF capacitor, the provided electrical energy by the triboelectric device is equal to W, which can be expressed as[2]

$$E_{electric} = W = \frac{CV_S^2}{2}$$

Where *C* represents the capacitance of the capacitor, and V_S represents the saturation voltage. Here, the achieved electric energy is $E_{electric} = 49\ \mu J$

When the ecoflex comes into contact with another film, the kinetic energy that is used as the triboelectric device's input energy is converted into electrical energy. Therefore, the kinetic energy will be[2]

$$E_{kinetic} = \frac{1}{2}mv^2 = 207.5\ \mu J$$

Here, $m =$ 1.08 g and $v = 0.6\ m/s$

Therefore, the mechanical energy conversion efficiency (η_{mech}) will be 23.6%.

S9. Influence of the different parameters on the device performance and optimization of the MOF concentration

the authors have investigated the influence of multiple factors, including dielectric constant, surface roughness, effective contact area, and interfacial adhesion, on the enhancement of the fabricated device. To examine the influence of dielectric effects, frequency-dependent dielectric measurement has been performed, as depicted in the figure S6(a). The results show that the dielectric constant of the Ni/Cu bimetallic MOF@PDMS layer is higher than bare PDMS over a frequency range of 0.5 to 25 kHz. The corresponding dielectric values indicate that the enhancement originates from dielectric polarization and microcapacitor network formation, which further contributes to increased effective capacitance and charge storage capability in the triboelectric layer. To evaluate interfacial charge retention, KPFM analysis

has been executed, as displayed in the figure S6(b) and (c). The bimetallic Ni/Cu MOF@PDMS exhibits a higher surface potential than bare PDMS, indicating enhanced surface charge retention due to the presence of the MOF. By these experiments, the MOF-assisted interfacial charge trapping sites are directly experimentally demonstrated, even though they do not measure trap depth or density. Furthermore, the charge transferred profile is examined, as shown in the figure S6(d). The presence of the bimetallic MOF@PDMS intermediate layer yields a better charge-transfer profile. Besides this, the pressure-dependent output voltages are measured under periodic finger tapping, as shown in the figure S6(e) and (f). The results reveal similar pressure-output trends for both devices, indicating that effective contact area is not the dominant factor. Therefore, the above-mentioned experiments conclude that the improved performance arises mainly from the synergistic effects of dielectric permittivity enhancement and interfacial charge retention.

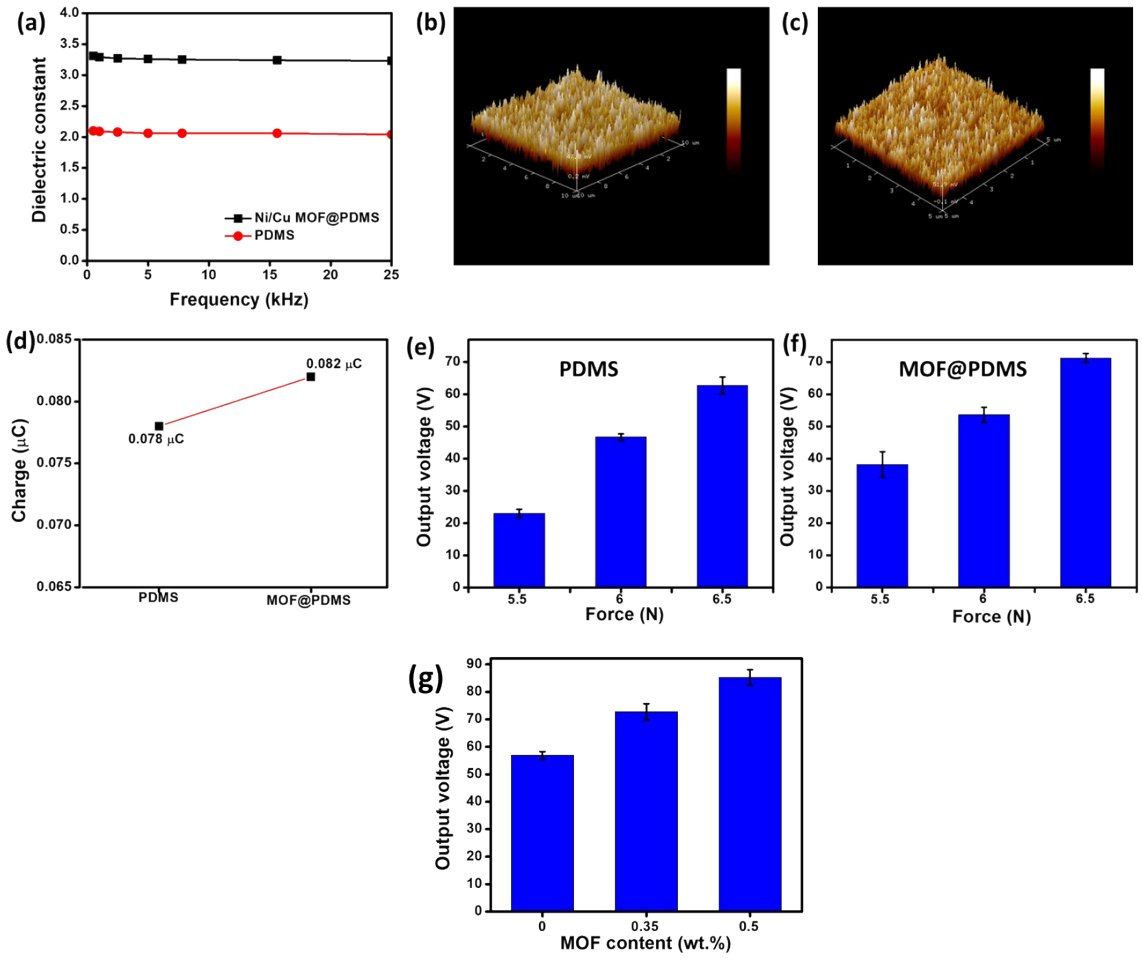

Figure S6: (a) Investigation of the dielectric values of the pure PDMS and Ni/Cu MOF@PDMS composite with respect to the frequencies ranging from 0.5 to 25 kHz.

Examining the surface potential of (b) PDMS and (c) Ni/Cu MOF@PDMS. (d) Monitoring the charge transfer profile of the triboelectric device with PDMS and MOF@PDMS layers. Monitoring the pressure-dependent output voltage of the (e) PDMS-supported triboelectric device and (f) MOF@PDMS supported triboelectric device. (g) Examining the effect of the different loading (0, 0.35 and 0.5 wt.%) of MOF nanomaterials on the output performance of the triboelectric device.

S10. Effect of the arch-shaped structure on the mechanical stability of the device

We have employed the idea of the fabrication of a spacer-free triboelectric device by adopting an arch shape during the design process. Therefore, the air gap is autonomously adjusted through the elastic deformation of the arch structure, rather than being constrained by a rigid spacer. When a human hand or foot presses the device, it undergoes reversible elastic compression, allowing precise contact-separation without applying excessive pressure on the triboelectric layers. In the releasing case, the elastic restoring force of the arch ensures a steady recovery of the gap. Besides this, the steady electrical output continued over 5000 cycles, establishing the mechanical durability of this spacer-free arch shape design, suggesting that the manual operation does not damage the integrity of the device.

S11. Comparison between the half-wave and full-wave rectification circuits and discussion on charge transportation in an electrolyte-free medium

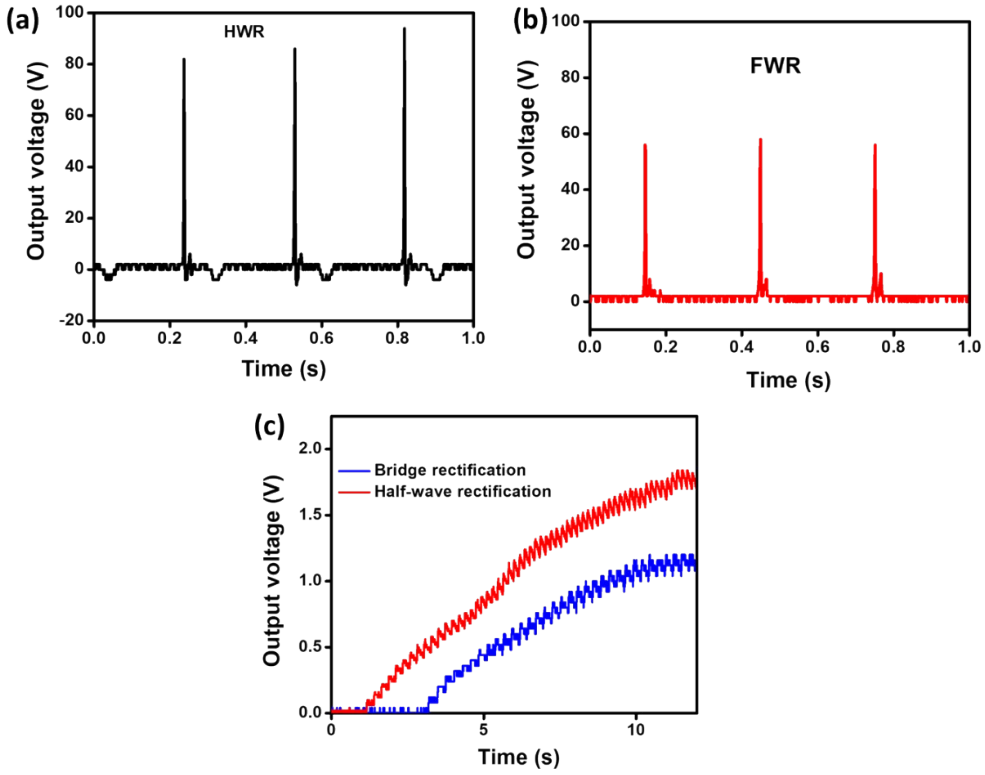

Figure S7: Investigation of the effect of the (a) half-wave and (b) full-wave rectifying circuit on the output performance of the triboelectric device. (c) Charging a 2.2 µF capacitor using a half-wave rectification process and bridge-rectifier.

Despite having very low conductivity, pure water is not completely non-conductive. Self-ionization of the water induces the ionic charge carriers.

$$2H_2O \rightarrow H_3O^+ + OH^-$$

At room temperature, this equilibrium results in a finite conductivity of ultrapure water with a value of 0.055 µS cm^{-1}, generating H_3O^+ and OH^- ions at 10^{-7} M concentration. Therefore, without the presence of any additional electrolytes, ionic conduction is maintained by these intrinsic ions. In this work, H_3O^+ and OH^- ions can electromigrate because of the applied pulsed electric field, generated by the fabricated triboelectric device. The transportation of charge occurs primarily via proton hopping, which works well under strong electric fields. Furthermore, the high electric field facilitates the charge transfers and augments ion availability through encouraging electric field double-layer formation and interfacial water dissociation. Therefore, the intrinsic ion production, field-assisted ion migration, and interfacial electrochemical processes ensure ionic conduction and charge transport in pure water. This

allows low-rate but noticeable electrochemical reactions without using any additional electrolytes.

S12. Discussion on the accumulation of local charge density at the graphite electrodes

The sufficient local charge density at the graphite electrodes is achieved through the pulsed electric output and output voltage of the triboelectric device. This is further combined with the cumulative charge accumulation at the electrode-water interface. Although the generated instant current remains low, each mechanical excitation creates a robust transient electric field that accelerates the charge injection towards the graphite surface. At the interface of the graphite-water, these charges are stored. From the ongoing mechanical reaction, the repeated pulsed charging creates a locally high effective overpotential. This gradually increases interfacial charge density and lowers kinetic barriers for HER at the cathode and OER at the anode.

S13. Discussion on the accumulated electrical energy to overcome the thermodynamic and kinetic barriers of water splitting

Without employing any current-boosting circuit or energy storage element, the intrinsic interfacial capacitance or EDL formed on the graphite electrodes effectively collects electrical energy at the electrode-water interface. The nanometre-scale capacitance at the graphite-water interface electrostatically stores the sporadic charges emitted by the triboelectric device's high-voltage and pulsed output. By continuously applying mechanical forces, the charge accumulation in the EDL gradually increases, leading to an enhanced interfacial potential and a strong electric field. For both HER and OER, this stored energy is sufficient to overcome thermodynamic requirements and reduce kinetic barriers. Therefore, water splitting is facilitated by time-integrated interfacial energy storage and field-driven reaction kinetics.

S14. Discussion on the reproducibility of the gas evaluation in electrolyte-free water splitting

Under the identical applied force, tapping frequency, electrode spacing, and water volume conditions, the approximately 30-minute onset time for observable gas evolution is consistent across experiments. Slight changes arise from the bubble nucleation and dissolved gas effects, which are common in an electrolyte-free setup. Pure water has a very low ionic conductivity.

This restricts electrochemical reactions from happening in a steady-state manner. This explains the delayed start and the ongoing rise in gas production over time, even with a steady mechanical input. Instead, the continuous electric field of the triboelectric device leads to a gradual accumulation of charge at the electrode-water interface, creating an electric double layer and accelerating water dissociation at the interface. Even with the constant applied force and frequency, the overall change in gas matches an accumulation-controlled, non-steady-state electrochemical process as the operation continues. This happens because of an increase in the time-integrated charge transfer.

References

1. Sarkar, D., Das, N., Saikh, M.M., Biswas, P., Roy, S., Paul, S., Hoque, N.A., Basu, R. and Das, S., 2023. High β-crystallinity comprising nitrogenous carbon dot/PVDF nanocomposite decorated self-powered and flexible piezoelectric nanogenerator for harvesting human movement mediated energy and sensing weights. *Ceramics International*, *49*(3), pp.5466-5478.

2. Mahanty, B., Ghosh, S.K. and Lee, D.W., 2025. Boosted triboelectric performance in stretchable nanogenerators via 2D MXene-Driven electron accumulation and $LiNbO_3$-assisted charge transfer. *Composites Part B: Engineering*, *291*, p.111995.

VS1: NCIL-TENG supported self-powered water splitting for hydrogen production.

Self-powered hydrogen production.mp4